



The structure of toluene-doped counterflow gaseous diffusion flames

Francesco Carbone, Alessandro Gomez *

Yale Center for Combustion Studies, Department of Mechanical Engineering and Materials Science, New Haven, CT 06477, USA

ARTICLE INFO

Article history:

Received 30 January 2012

Received in revised form 10 May 2012

Accepted 11 May 2012

Available online 14 June 2012

Keywords:

Counterflow

Diffusion flame

Toluene

Chemical kinetics

ABSTRACT

The structure of gaseous counterflow diffusion flames perturbed with the addition of hundreds of ppm of prevaporized toluene is studied in two distinct flame environments: a blue methane flame stabilized on the *fuel* side of the gas stagnation plane and an incipiently sooting ethylene flame stabilized on the *oxidizer* side. The goal is to provide a well-defined testbed in terms of temperature–time history, major species and part of the radical pool, for the examination of reference fuels that are critical components of practical fuel blends. Gas samples are extracted from the flame with fused silica microprobes for subsequent GC/MS analysis and thermocouples and thin filament pyrometry are used to characterize the temperature field. Profiles of critical toluene pyrolysis products and stable soot precursors are compared with computational models using two semi-detailed chemical mechanisms. Results show that in the methane flame some oxygen containing radicals like O and OH are contributing early on to the toluene destruction path. In the incipiently sooting ethylene flame, the primary attack is from H alone. This finding confirms the different challenges that such flames pose to the validation of a chemical kinetic mechanism. The onset of toluene decay in these flames begins at relatively modest temperatures, on the order of 800 K. This reactivity is captured reasonably well by both chemical mechanisms in the methane flame, in the absence of reactants larger than C₂, but not so in the ethylene flame, in the presence of a richer, more complex mixture. The aromatic ring opening mechanisms are not adequately modeled in either case. This discrepancy has implications for the modeling of practically relevant fuel blends with both aliphatic and aromatic compounds. The dominant species larger than toluene in the doped methane flame is ethylbenzene, which at least one of the mechanisms reproduces quite well. The largest measured species in the incipiently sooting flame is indene, whose concentration increase due to toluene addition is properly captured by one of the models. The experimental dataset reported here may help identifying future improvements to chemical kinetic mechanisms and complement other reactor datasets lacking the coupling of kinetics and transport of flame environments.

© 2012 The Combustion Institute. Published by Elsevier Inc. All rights reserved.

1. Introduction

A considerable fraction of the world's energy consumption entails the use of transportation fuels, comprising hundreds of aromatic and aliphatic components [1]. Since studying their chemical kinetic behavior is a daunting and unrealistic challenge, recent trends in the research community have been focused on the establishment of surrogate fuels, consisting of as few as two and as many as fourteen constituents, that are formulated to mimic some predefined combustion performance parameters [2–9]. The emphasis in the formulation of these surrogates is aimed at capturing overall combustion properties, such as ignition delay, extinction strain rate and threshold sooting index, among others. Several efforts were focused on the modeling of the chemistry of

surrogate components as well as improving surrogate performance in reproducing real fuel behavior. The topic has been reviewed in Refs. [10–13]. However, testing in well-defined and well-controlled flames to establish the chemical kinetic behavior of these complex fuel blends and their interplay with transport is necessary to deepen our understanding of the chemical kinetic coupling of the various fuel components. More generally, the characterization of the chemical behavior in flames of an important class of reference fuels such as the aromatics, that are invariably present in transportation fuels, is necessary. Among aromatics, toluene is a primary reference fuel present in both real fuels and their surrogates [1,9,14] and its chemistry is of relevance to the decomposition of larger aromatics.

Brezinsky and coworkers performed pioneering experiments on toluene oxidation in a flow reactor [15]; Colket and Serry [16] investigated toluene pyrolysis in a shock tube; several studies followed later on with a focus on the chemical characterization of toluene consumption [17–23]. To date there have been only a few studies on toluene chemistry in flames, namely, counterflow air/li-

* Corresponding author. Address: Department of Mechanical Engineering and Materials Science, Yale University, P.O. Box 208286, New Haven, CT 06520-8286, USA. Fax: +1 203 432 7654.

E-mail address: alessandro.gomez@yale.edu (A. Gomez).

quid pool flames [24], laminar coflow diffusion flames [25] and, more recently, low-pressure premixed flames [26–28]. The diffusion flame studies were conducted in the presence of significant soot load with all the attending complications. Furthermore, no comprehensive modeling of toluene high-temperature chemistry was available at the time. A systematic investigation of the structure of toluene-doped flames in a broad range of conditions for the validations of emerging chemical mechanism is still missing.

By using gas sampling and chemical analysis, a comprehensive investigation was conducted on the detailed flame structure of a blue (nonsooting) methane counterflow diffusion flames and of an incipiently sooting ethylene one, both perturbed by trace amounts (on the order of hundreds of ppm, molar) of toluene. As elaborated in previous work of our group [29–31], the rationale for using a counterflow flame environment with a baseline flame perturbed by the fuel under examination is that it can be regarded as a flow reactor that, although not as well controlled as typical chemical kinetic laboratory systems, such as shock tubes and stirred reactors, can nonetheless provide a well-defined environment in which the coupling of transport and chemical kinetics takes place. The temperature–time history can be easily adjusted to be virtually identical for both doped and undoped flames by varying the strain rate and the feed stream composition. Furthermore, major species, critical radicals and some C1–C4 intermediates are fixed by the baseline gaseous reactants. This feature is particularly attractive and may mimic another aspect of jet fuel combustion, with less stable and/or more volatile hydrocarbons that are part of the fuel blend contributing to the establishment of the reactive environment. The doped approach may result in an enhancement of reaction pathways of the added reference fuel that are significant when it is mixed with other hydrocarbons and may be inactive when it is used alone. Also, it minimizes the potential for vapor condensation, since the condensable species are at very small concentrations.

The selection of the experimental conditions is aimed at spanning a broad range of values of the stoichiometric mixture fraction, encompassing both nonsooting and incipiently sooting conditions, with the flame positioned on either side of the gas stagnation plane, similarly to the work of Sun et al. [32]. Therefore, the chemical environment in which toluene pyrolytic destruction and subsequent hydrocarbon growth chemistry take place is rather distinct in two sets of flames and provides a challenging testbed for the validation of chemical kinetic mechanisms.

With respect to the latter, we supplemented the experimental study with computational modeling of the flames using the OPP-DIFF solver [33] with different chemistry mechanisms [34–37] for comparison with the experimental results of the toluene-doped flames.

2. Experimental setup

The experimental system was described in detail in previous work from our laboratory [29–31]. Briefly, a counter flow burner is used, including a nitrogen shroud that shields the flame from room drafts and ensures burning in the controlled atmosphere that is determined by the composition of the feed streams. The inner diameter of the fuel and oxidizer outlets is 12.5 mm and the burner separation is 14.1 mm. At the small liquid flow rates of interest, a syringe pump is used to feed an electrospray dispersing the liquid fuel in the preheated fuel/nitrogen stream [38]. To prevent condensation downstream of the electrospray unit, PID controllers keep the fuel line at 435 K, which is well above the dew point of the dopant/ $\text{CH}_4/\text{C}_2\text{H}_4/\text{N}_2$ mixtures. Gas samples are extracted from the flame through a microprobe, consisting of a small silica probe with an outer diameter of 360 μm and an inner diameter of 150 μm . The

sampling system is kept at a constant temperature of 423 K. Previous experiments showed that the use of finer probes did not modify the species profiles appreciably [29–30].

The chemical analysis is performed by a gas chromatograph (Agilent 6890A) equipped with mass spectrometer (MSD, Agilent 5973N), thermal conductivity (TCD), and flame ionization (FID) detectors. The instrument is capable of quantifying complex hydrocarbon mixtures, CO , CO_2 , O_2 and N_2 . It uses two capillary columns, a Supelco Carboxen and an Agilent HP-1, connected to the FID and MSD, respectively. In addition, the TCD measures non-hydrocarbon stable gases separated by means of a third column (Alltech, Packed Molecular Sieve). A homemade nickel-based catalytic converter (Methanizer) allows for FID quantification of CO and CO_2 upon their conversion into methane in the presence of hydrogen. The system can separate and quantify O_2 , CO , CO_2 , light gaseous hydrocarbons and higher hydrocarbons up to at least C14.

Species are identified during the GC/MS data post-processing by both the column retention time and the molecule-specific mass spectrum. Since FID and MS analyses are time consuming, a semi-automated chemical analysis method is employed that consists of sampling the gas and storing it in a battery of 16 heated sampling loops at an absolute pressure of 300 Torr and at $T = 423 \text{ K}$. The stored samples are injected for the analysis by a computer-automated sequence driving two pneumatic-actuated injection valves and two electro-actuated multiposition valves (Valco), so that samples are automatically analyzed overnight [29–31,39–41]. An optimized time–temperature program for the chromatographic columns keeps the total analysis time at a minimum.

The accuracy in the GC/MS analysis and the reproducibility of the data are ensured by repeated sampling at the same position in the flame, scanning the flame in the two opposite directions. Each flame is scanned at least three times, twice starting from the fuel side of the burner once from the oxidizer side. This procedure is implemented for two reasons: the species may suffer from condensation and/or aging in the sampling/storing system; and, minor, and often inevitable, leaks between adjacent loops connected to the multiposition valves may result in sample modification during the analysis and profile distortions. These leaks would affect the signal of the more abundant species when their concentration is significantly different in adjacent loops and in the presence of pressure difference. The latter problem is circumvented by equalizing the pressure between adjacent loops during sampling, injection and analysis and by refining the scanning in the presence of large concentration gradients. These potential artifacts would have led to lack of reproducibility because the sample “history” would be dependent on the scanning direction. The modest scatter of the measured concentration profiles among the various scans (see below) attests to the absence of these potential problems. Additional checks are performed occasionally by analyzing the gas at selected flame points on the fly, that is, by bypassing the storage system to ensure that sample aging is not occurring.

Standard gases (Scotty®) are used for calibration of light gaseous species (up to C5 species). Aliquots of liquid hydrocarbons dissolved in normal-decane are electrosprayed in the fuel line and vaporized in hot nitrogen, much the same way as toluene, for the calibration of heavy liquid hydrocarbons. The calibrating mixture is sampled through the same capillary used for flame scans and stored in the multiposition valves before being analyzed. The total relative error in measured concentrations is estimated at $\pm 10\%$ for light species and $\pm 15\%$ for the heavier ones by considering the uncertainties associated with calibration, sampling and analysis procedures.

Temperature measurements are performed in two ways: in the first, a flame-welded, silica-coated Pt-10%Rh/Pt thermocouple is

used with an approximately cylindrical junction measuring 70 μm in diameter. In the second, gaseous temperatures between 1200 K and 2300 K are measured via Silicon–Carbide (COI Ceramics, Inc.) thin filament pyrometry [42] by using a digital camera (Canon EOS 40D) with a 70 mm f/5.6 lens in the visible range. The technique is calibrated by immersing a SiC wire in the post flame region of a flat premixed flame, as described in [43]. Standard corrections for radiative losses are applied to both techniques by considering heat transfer of cylinders in a cross flow [44]. The estimated uncertainty in the measured temperatures is at ± 50 K, after combining various errors.

The reason why the temperature is measured by two independent techniques in the most critical temperature range is that preliminary measurements indicated significant discrepancies between computational model and measurements even in the baseline gaseous flames, especially the ethylene one. We will elaborate more extensively on this discrepancy in the Section 5. By using the thin filament in the second technique we minimized the intrusiveness of the measurement. In fact, no perturbation of the wire to the flame was detected either by naked eye, or by using the camera and a cathetometer, which is not surprising since the wire diameter measures only 13 μm , that is less than 1/5 of the thermocouple size used in the other measurement set.

Since multiple temperature and species scans are performed and since these scans will have to be superimposed to one another and compared with the computational results, one needs to “register” axial coordinates with respect to some reference point. One such a reference point is provided by the blue chemiluminescent layer of the flame that can be accurately identified experimentally using either a cathetometer or the digital camera in each flame. This approach is preferable to using one of the boundaries since depth of field and visual obstruction from the burner housing make the measurement somewhat more challenging and because the flame position with respect to the burner outlets may be affected by probe intrusiveness. The accuracy in recording such position with respect to the boundary of the domain on the fuel side is estimated at ± 0.1 mm and ± 0.2 mm for the methane flames and the ethylene flame, respectively. The larger uncertainty in the ethylene flame position is associated with the presence of the soot layer. The position of the blue layer is recorded also in the presence of each probe, which provides an estimate of the disturbance introduced by the probe, in addition to a convenient reference to superimpose all measurement profiles unambiguously. The presence of the silica probe causes a flame displacement estimated at less than one mm for the methane flames and less than 0.4 mm in the ethylene flames, which are of the same order as the 0.6 mm estimated by OH PLIF in Ref. [30], whereas the presence of the thermocouple causes a shift of at most 0.6 mm in the methane flame and less than 0.2 mm in the ethylene flame. No observable displacement is detected in the presence of the thin filament. Importantly, any necessary shift for the superposition of a particular flame scan with another one is quantified and performed once for all species and profiles; that is, no additional unjustifiable shifts of individual species profiles is made to “improve” consistency among datasets.

3. Computational modeling

The experimental study is supplemented with computational modeling of the flames using the OPPDIFF solver [32], included in the software package Chemkin Pro (Reaction Design). Details of the model formulation will not be discussed since this software package has been widely used in the combustion community for some time. With respect to the chemistry mechanism, we used GRI-Mech 3.0 [34] to describe the baseline flames, the mechanism recently developed by Metcalfe et al. [35], in short Metcalfe-Mech,

and the high-temperature version of the semi-detailed mechanism for large hydrocarbons developed by Ranzi et al. [36,37], in short Ranzi-Mech. The GRI-Mech mechanism is used to describe the baseline flames as a reliable chemical kinetic model including C1–C2 chemistry. The Metcalfe-Mech was chosen for comparison with the experimental results as the most recently developed and broadly validated mechanism for toluene oxidation and pyrolysis. It includes 329 species and 1888 reversible reactions. The Ranzi-Mech, on the other hand, is more ambitious, including both aromatics and aliphatics typically present in jet fuel surrogate, up to C16 species, and growth species of relevance to soot formation, some of which are also included in our experimental dataset. It includes 250 species and 7683 elementary reactions. The last two mechanisms were designed to properly degenerate to validated sub-mechanisms for C1–C4 hydrocarbons, in the absence of larger species, so that they can be used also for the modeling of the baseline flames. Preliminary numerical results for the Ranzi mechanism were also obtained using the solver openSMOKE for laminar opposed-jet flames developed in Ranzi's group [45], since it converges much faster when dealing with their large chemical kinetic mechanisms than Chemkin Pro. Numerical results were obtained on adaptive grids each consisting of more than one hundred seventy points. Multicomponent diffusion coefficients and thermal diffusion were accounted for in the transport model, but had marginal effects on the results, as compared to using the mixture averaged transport coefficients. This is not unexpected since the most abundant species come from the baseline flames as a consequence of the doping approach.

4. Flame composition

Two sets of flames are examined: a blue methane flame is stabilized with a value of the stoichiometric mixture fraction, z_f , of 0.79, with $z_f = 1/(1 + sY_{FF}/Y_{OO})$, where s is the stoichiometric mass ratio of oxygen to fuel, Y_{FF} and Y_{OO} are the feed stream mass fraction of the fuel (regardless of the chemical composition) and oxygen, respectively. This flame is established on the *fuel* side of the gas stagnation plane. In a second set of flames, incipiently sooting conditions are established in an ethylene flame stabilized on the *oxidizer* side of the gas stagnation plane, corresponding to a value of the stoichiometric mixture fraction of 0.19. Table 1 specifies the boundary conditions (mole fractions, total mass flux and outlet temperatures of both fuel and oxidizer streams) for the four flames under consideration. Trace amounts of an ethane impurity in the C_2H_4 supply were revealed by chromatographic analysis and are also listed in the table, in addition to the values of z_f and of the density corrected strain rate, $a = \frac{2V_{ox}}{L} \left(1 + \frac{V_f \sqrt{\rho_f}}{V_{ox} \sqrt{\rho_{ox}}} \right)$, where V_{ox} and V_f are the mass average velocity at the oxidizer and fuel boundaries, respectively, L is the burner separation, and ρ_{ox} and ρ_f are the densities of the mixture at the boundaries [46].

The methane flame and ethylene flame are doped with 440 ppm and 865 ppm of toluene, respectively. The dopant concentration is chosen on the basis of two considerations: (1) it should be sufficiently small so as not to change the overall flame structure and (2) it should be sufficiently large so that the dopant contribution to the production of critical species can be discriminated from the contribution of the baseline flame. As a result, cause-and-effect relationship of the perturbation can be established. The addition of even such a small fuel amount increases the peak temperature by 20–30 K and the flame location shifts slightly toward the oxidizer side. To preserve the temperature–time history and ensure comparable Arrhenius kinetics between flame pairs, the temperature profile needs to be the same in all of them. Also, since the mixture fraction is, in the first approximation, a single-valued (complemen-

Table 1
Flame boundary conditions.

	CH ₄ Baseline	CH ₄ Toluene	C ₂ H ₄ Baseline	C ₂ H ₄ Toluene
<i>Fuel side</i>				
Molar composition				
N ₂	0.897	0.899	0.728	0.730
CH ₄	0.103	0.100		
C ₂ H ₄			0.272	0.268
C ₂ H ₆ impurities	<30 ppm	<30 ppm	<300 ppm	<300 ppm
Toluene		440 ppm		865 ppm
Mass Flux, g/(cm ² ·min)	2.80	2.87	1.62	1.65
Temperature, K	435			
<i>Oxidizer side</i>				
Molar composition				
N ₂	0.227	0.814		
O ₂	0.773	0.186		
Mass flux, g/(cm ² ·min)	3.19	3.29	1.89	1.91
Temperature, K	380			
Strain rate, s ⁻¹	154	158	93.4	94.6
z_f	0.79		0.19	

tary error) function of the axial position, fixing its value ensures that the flame position is unaltered by the perturbation. To maintain the same temperature profiles as in the baseline flame, we increased the inert mole fraction in the fuel stream, which lead to a small change in z_f and a further shift of the flame towards the oxidizer side. We compensated for this shift by a small increase in both the oxidizer and, to a lesser extent, the fuel flow rates.

5. Results and discussion

5.1. Temperature Profiles: discrepancy between models and experiments

Figure 1 shows the measured temperature profiles for both baseline flames. As for all the subsequent figures, the methane flames are presented on the left and the ethylene flames on the right, for a side by side comparison of the two flame conditions. Raw measurements profiles are consistent with one another but there can be a scatter as large as ± 50 K, mostly at the highest temperatures. In addition to notorious uncertainties associated with the radiative correction, the most significant source of error is associated with the intrusiveness of the technique. Flame/thermocouple interaction results in flame displacements that undoubtedly altered the profile. To estimate the error associated with this effect, the flames are scanned in both directions, to maximize the scatter of the reported data, as discussed earlier. In the region between 7 mm and 8 mm of ethylene flames, we observed a small hysteretic behavior of the probe with different readings depending on the direction of the scan. The behavior was more pronounced in the

thermocouple measurements as compared to the thin filament pyrometry, consistently with the respective intrusiveness of the techniques.

Corrected temperatures are also shown in Fig. 1 and they are in good agreement with one another independently of the measurement technique and of the probe size. The implication is that the temperature field is well characterized since it was established with two essentially independent techniques. The temperature of the toluene-doped flames (not reported here) was measured only by thermocouples after this initial validation and is virtually indistinguishable from that of the baseline flames.

The computational results in the figures are obtained using all three chemistry mechanisms and the boundary conditions reported in Table 1 [34–37]. Metcalfe-Mech [35] and Ranzi-Mech [36,37] should degenerate to the methane chemistry of the GRI-Mech 3.0 [34], with small corrections for some minor species. As far as temperature, all models produce virtually indistinguishable results as represented with a single line in Fig. 1 for both baseline and doped flames. Comparing model and measurements in the methane flame, one observes that they agree with respect to the general shape and position of peak temperatures, but the experimental profile is broader than the computed one and the measured corrected peak temperature is higher than the computed one. These results appear to contrast with the excellent agreement reported in [47] using nonintrusive Raman spectroscopy and differ from the thermocouple data of [48] that showed narrower profiles than the computed ones. However, in the first case the strain rate was reportedly treated as an adjustable variable to align computation and experiments. Turning to the ethylene base flame, we

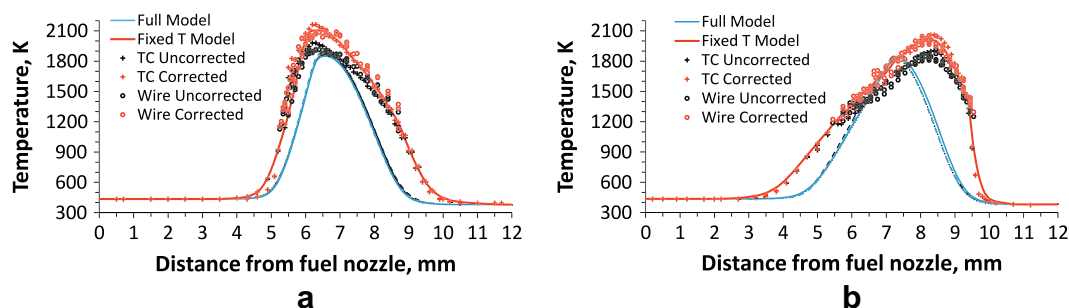


Fig. 1. Comparison of experimental measurements, via either thermocouple or thin filament pyrometry, and computation results of the temperature profiles in the baseline methane flame (left) and in the ethylene baseline flame (right). The computational results obtained with three chemistry mechanisms (see text) and for the baseline and the doped flames, are indistinguishable.

notice that the discrepancy is more significant and affects also the shape of the profile, with the modeling yielding essentially symmetric profiles in contrast with the experiments exhibiting a “shoulder” on the fuel side. Even the position of the maximum temperature is evidently shifted towards the oxidizer side for the experimental data. Discrepancies between model and measured temperatures in ethylene diffusion flames were previously reported [49]. In view of this disagreement and the sensitivity of Arrhenius kinetics to temperature for the high activation energy chemistry of interest, we decided to use in the model the properly smoothed temperature profile that had been experimentally measured, and sidestep this discrepancy by dropping the energy equation in the flame model.

Figure 2 shows the axial velocity and the CH concentration profiles obtained with the fixed-temperature model compared to the one predicted solving the full system of equations including the energy equation. When comparing the experimental results with the computational ones, the position of the blue chemiluminescence, previously used to overlap the experimental profiles to one another, was found to be approximately halfway between the CH and OH maxima predicted by the fixed-temperature model and the concentration profiles of major species reasonably agree with the computed ones (see below). For the methane flames we notice that the full model predicts a location of stagnation plane and CH peak that are shifted 0.35 mm to the oxidizer side with respect to the fixed-temperature results. There is also an accompanying distortion of the velocity profiles mostly on the oxidizer side (8 mm or more from the fuel nozzle). As a result, since toluene and methane decomposition occurs on the fuel side, the predicted concentration profiles are not significantly affected except for this shift. With respect to the ethylene flames, imposing the experimental temperature profile in the computations does not significantly change the predicted flame position but affects the axial velocity profiles on *both* sides of the stagnation plane, so that the effect of the temperature discrepancy influences the entire flame structure, with the exception of the zone between 5.8 mm and 7.3 mm, where many of the reactions of interest occur (see below). To be consistent in the comparison of flame sets and to avoid excessive data cluttering in the figures, only results of the fixed temperature model are reported in the ensuing discussion.

The need for profile shifts and the observed distortion as compared to the full model solution are likely to be not only associated with probe disturbance, but also with two additional effects: first, the velocity profile at the boundary may be in part responsible for disagreements and one would have to measure the gradient at the boundary, which was not done in the present work; and second, the use of a shroud flow to shield the flame from room disturbances may drag the flame slightly from its original position, which cannot be taken into account in the one-dimensional model. In the end, conclusions to be drawn will not be affected by these artifacts.

If one considers CH as a provisional marker of the reaction zone, Fig. 2 confirms that the methane flames are stabilized on the *fuel* side of the stagnation plane whereas the ethylene flames are stabilized on the *oxidizer* side, consistently with the expectations in the selection of the mixture fraction values in the two sets of flames.

5.2. Overall structure of the flames

The overall structure of the investigated flames is shown in Fig. 3 in terms of normalized total carbon count, oxygen and C1–C2 species profiles both determined experimentally and computationally. The normalized total carbon count is compared with the computed mixture fraction based on carbon atom conservation. Good general agreement is observed, attesting to (a) the success of the approach in generating a well-controlled reactive pool in which toluene consumption occurs and (b) the capability of chemistry mechanisms that were developed for larger hydrocarbons to describe the chemistry of small hydrocarbons (C1–C2) flames. Experimental profiles are on average only slightly broader than the numerical ones, probably as a consequence of the different intrusiveness of thermocouple and gas sampling probe. The main disagreement between experimental and modeled data is observed for the methane flame with respect to the methane concentration profile for values of the abscissa ranging from 3.5 mm and 4.5 mm. In this zone the experimental methane signal unexpectedly drops even if the concentrations of all the other species are negligibly small, suggesting that there is no ongoing chemistry. The loss also affects the total carbon count showing a dip of about 20% in the same zone. The reason for this systematic loss in carbon signal in

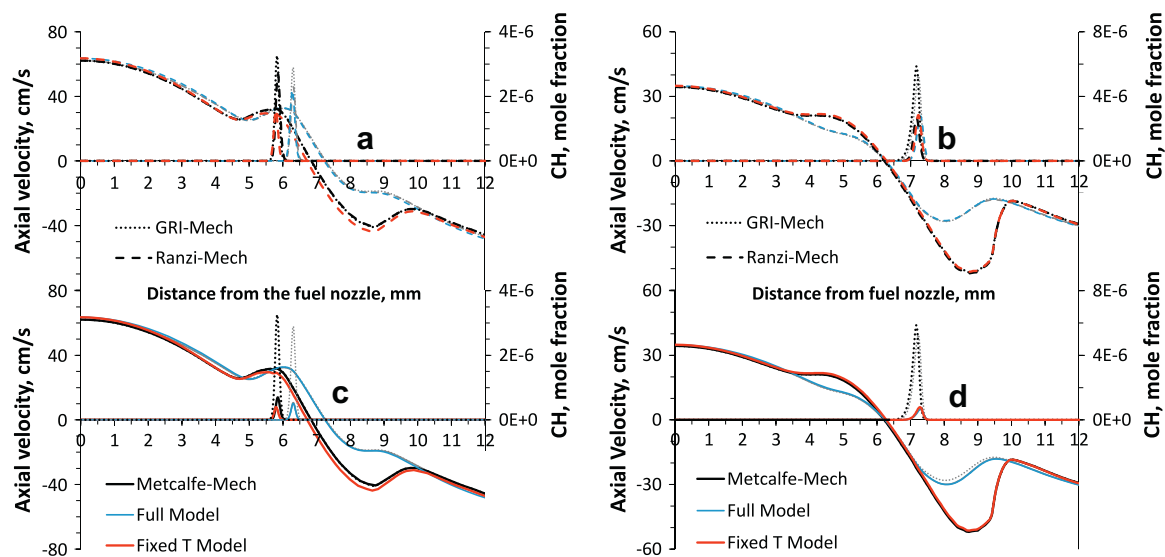


Fig. 2. Computed axial velocity (left ordinate) and CH mole fraction (right ordinate) profiles in the methane flames (left) and in the ethylene flames (right). Computational results for the fixed temperature solution (red and black lines), using the experimentally measured temperature profile as input to the model, are compared with the full solution (blue and gray lines), including the energy equation. Colored lines are for the doped flame whereas gray-scale lines are for the baseline flames. GRI-Mech results are shown for comparison with those from Ranzi-Mech [36] (top panels, a and b) and from Metcalfe-Mech [35] (bottom panels, c and d). (For interpretation of the references to color in this figure legend, the reader is referred to the web version of this article.)

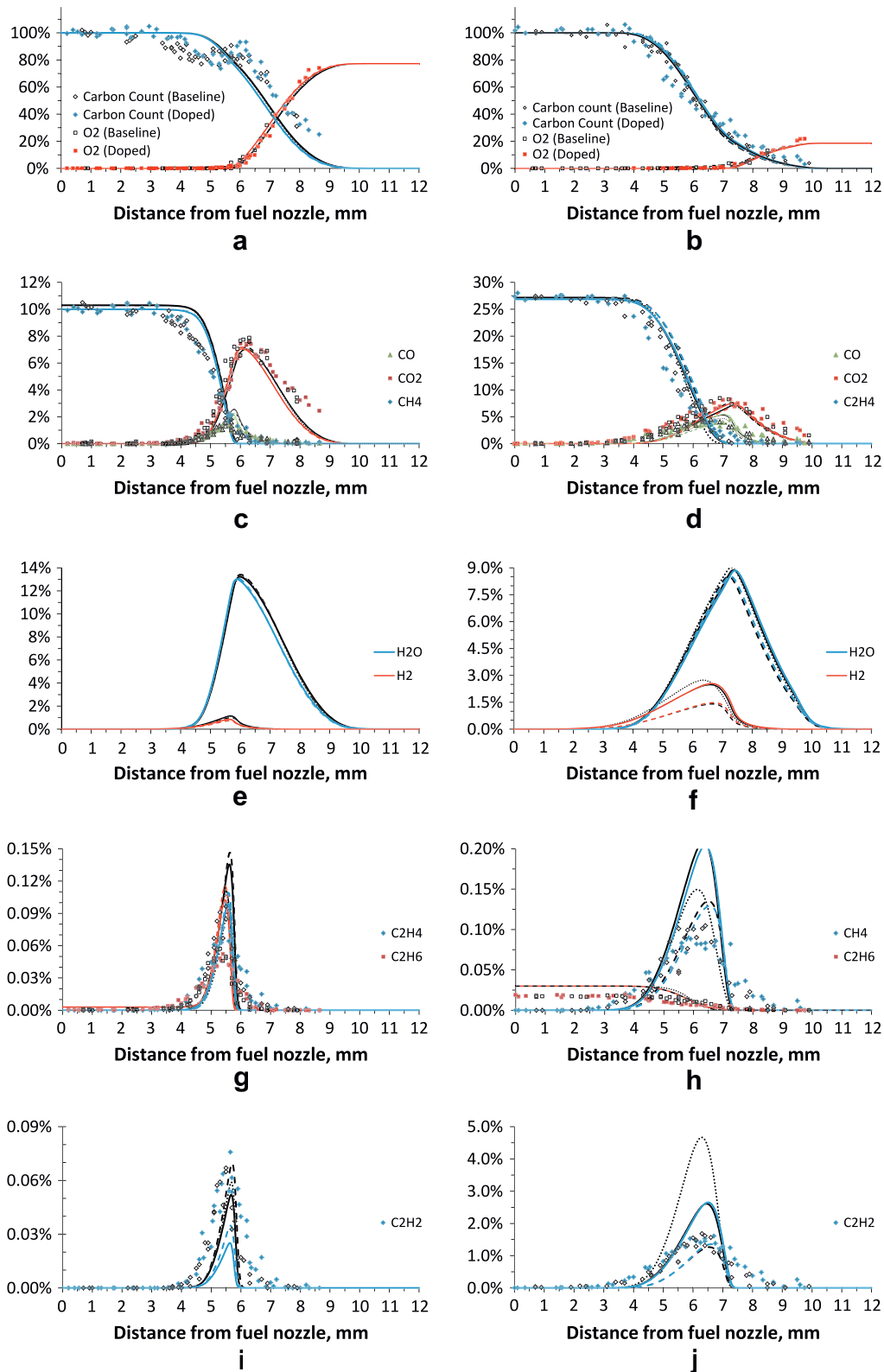


Fig. 3. Comparison of profiles of carbon count/mixture fraction and major species(a–f), and C2 species (g–j) between baseline flames (black open symbols) and doped ones (full colored symbols) for methane flames (left column) and ethylene flames (right column). The computational results, when distinguishable, are plotted with the same legenda as in Fig. 2, that is, colored lines for doped flames, black lines for baseline flames, continuous line for Metcalfe-Mech [35], dashed line for Ranzi-Mech [36] and dotted line for GRI-Mech 3.0 (just in the case of the baseline flames) [34]. (For interpretation of the references to color in this figure legend, the reader is referred to the web version of this article.)

this region is not clear. In additional experiments, we observed that the drop in carbon count occurs when part of the probe conduit crosses the hot region at the periphery of the flame, becoming lo-

cally slightly incandescent, even if the probe tip is still in the cold zone of the combustion region. This effect is in part a consequence of relatively low strain rate in the shroud region, causing the flame

to be thicker in that region. After slightly bending the probe to avoid this local heating, the drop in carbon count disappeared. At any rate, the methane flame reactivity in the region affected by the loss in carbon signal is negligibly small so that this signal drop will not significantly affect the result interpretation. Notice that this artifact does not affect the ethylene flame, since the flame is stabilized on the oxidizer side of the stagnation plane and the cold region on the fuel side can be completely scanned with the probe conduit never developing hot spots.

The reactive zone in the methane flames approximately extends from 4.5 mm to 7.5 mm from the fuel nozzle. Model results are in good agreement with one another and with experimental results. They predict reasonably well the methane consumption slope, if one accounts for the effect of the probe intrusiveness on the resolution of the steep slope, and show good agreement in terms of CO, CO₂, oxygen concentration profiles, only carbon monoxide being slightly overpredicted.

The reactivity in the ethylene flames spreads over a wider region, extending from 4 mm to 9 mm from the fuel nozzle, partly because of the smaller strain rate of those flames as compared to the methane ones. Also in this case, all models are able to predict reasonably well CO, CO₂, oxygen concentration profiles and ethylene consumption.

The computed mole fractions of stable species H₂O and H₂ are also shown in the figure without any experimental values for comparison. The results of the models are all consistent with each other, with the exception of the hydrogen profiles in the ethylene flames for which Ranzi-Mech predicts a peak concentration half as large as the value of the other two mechanisms. Significant amounts of water vapor and molecular hydrogen are present in the regions where toluene consumption occurs for all the investigated flames.

Turning to C1 and C2 intermediates, we observe that the addition of toluene does not change the concentration of these species that are mainly the result of the primary gaseous fuel chemistry, and that GRI-Mech, Metcalfe-Mech and Ranzi-Mech yield similar results. Ethylene is well predicted by all models in both flames, whereas ethane shows a disagreement in the maximum concentration by a factor of two in the methane flames. The methane profile in the ethylene flames is well captured by Ranzi-Mech, whereas GRI-Mech and Metcalfe-Mech predict a larger peak concentration by a factor as large as two. With respect to acetylene, all models underpredict the acetylene concentration peak by approximately 50% in the methane doped flame, whereas they correctly predict the profile for the baseline methane flame. In the ethylene flames the experiments are in better agreement with Ranzi-Mech, with Metcalfe-Mech overpredicting the peak concentration by 50% and the worst disagreement unsurprisingly [34] brought about by the GRI-Mech 3.0 with a factor of three overprediction.

Comparing the two flame environments, we notice that in the ethylene flames: (a) gradients are shallower than in the methane flame, as a consequence of the lower strain rate; (b) the CO/CO₂ and H₂/H₂O peak mole fraction ratios are larger, (c) the concentration of C₂H₂, a critical species in soot production, is also much larger than in the methane flame. These quantitative differences suggest that the fuel degradation occurs in an oxygen-deficient environment in the ethylene flame as compared to the methane one. This finding is not surprising in view of the relative position of the flame and the stagnation plane, with the flame located further on the oxidizer side of the gas stagnation plane in the ethylene flame and also because of the incipient sooting conditions of that flame. These considerations apply also to toluene degradation, as discussed in the next section.

5.3. Tracking toluene pyrolysis

Figure 4 shows the concentration profile of toluene in the investigated flames. No toluene was detected in the blue baseline meth-

ane flame, whereas about 6 ppm of toluene were identified in the incipiently sooting ethylene flame (notice the different scale in Fig. 4b). A progressive toluene signal decrease of about 20% was observed for values of the abscissa ranging from 3.5 mm up to 4.5 mm in the doped methane flame. As for the methane concentrations, this drift in signal does not correspond to toluene consumption, since no other species were detected in this zone in significant concentrations (see below). The decrease is tentatively attributed, as for the methane baseline flame, to a sampling artifact. After this signal loss, toluene concentration suddenly drops between values of the abscissa of 4.5 mm and 6 mm, being almost totally consumed at the end of this range. The predictions of both models are almost coincident, closely approximating the slope of toluene decay in this zone. The modeled toluene concentration slightly increases with respect to the boundary value right before the consumption zone. This behavior is the result of including simultaneously thermal diffusion and multicomponent transport in the computation.

With respect to the doped ethylene flame, experimental data show a smooth toluene concentration profile gradually decaying to zero in the zone between 4.5 mm and 7.5 mm from the fuel nozzle outlet. The loss in signal reported for the doped methane flame was not observed in the doped ethylene flame. Also in this case, the two models give almost equivalent results for the toluene concentration profile. Similarly to the methane flame case, the models predict a slight overshoot of toluene concentration with respect to the boundary value, preceding its consumption, which is attributed to transport effects. The computed concentration decay is more abrupt than the experimental one, beginning at about 5 mm from the fuel outlet. At first glance, this macroscopic discrepancy would appear troublesome. It suggests a much greater reactivity in the experiment. But, on second examination, this discrepancy is consistent with the reported increased reactivity of toluene/iso-octane mixture at temperature larger than 1100 K with respect to that of the individual hydrocarbons [21,50]. Such an effect depends on the interaction between iso-octane fragments and toluene and cannot be reproduced by any of the existing models [51]. Such fragments are already present in the ethylene baseline flame starting from the location at 4 mm from the fuel nozzle (see below), as result of ethylene pyrolysis. Toluene itself is generated in this zone in the ethylene baseline flame and both mechanisms largely overpredict its concentration, the discrepancy being larger for the Metcalfe-Mech as compared to Ranzi-Mech. We tentatively conclude that these discrepancies are consistent with previously reported results and suggest possibly missing steps in the initial pyrolytic consumption of toluene in both mechanisms.

The experimental and computational concentration profiles of C3–C6 species are summarized in the rest of Fig. 4. Numerical results include only those with Metcalfe-Mech and Ranzi-Mech, since the GRI-Mech 3.0 model does not consider species larger than C2, except for propane. Species smaller than toluene can be generated either as consequence of toluene cracking, or by the chemistry of the baseline flames. Consequently, when detected, their concentrations in the baseline flame are also reported to distinguish between the two contributions and complete the description of the chemical “pool” in which toluene decomposition occurs.

With respect to C3 species, we detected propene, propyne and allene, but the GC–MS configuration and temperature programming did not allow us to discriminate between the last two. So, the measured concentrations of a generic C₃H₄ are compared to the sum of predicted propyne and allene concentrations. Propane was detected in negligible amount at less than 1 ppm in all investigated flames, even though the models predict concentration as high as 10 ppm (5 ppm) in both the baseline and doped methane (ethylene) flames. In the doped methane flame, the maximum con-

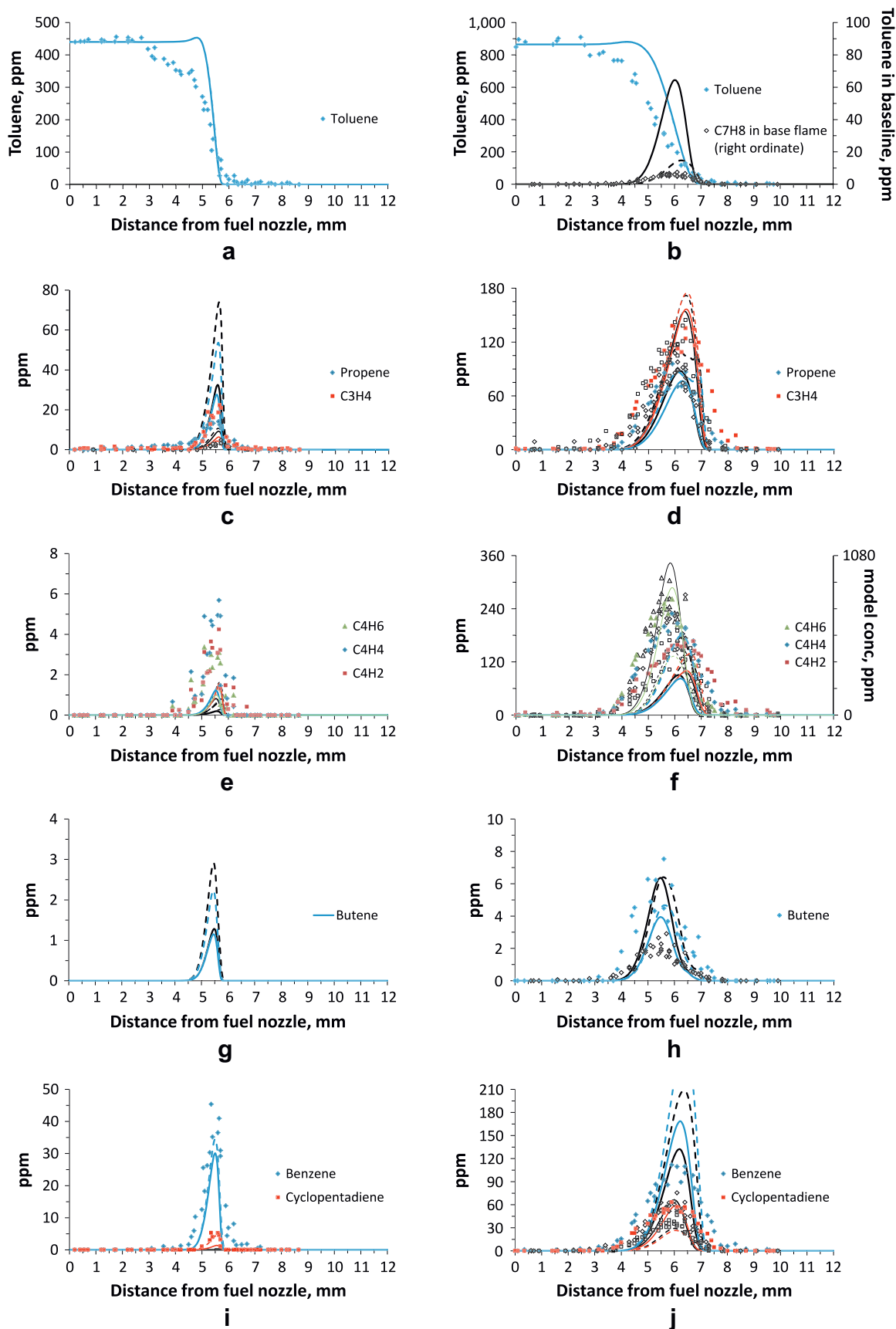


Fig. 4. Comparison of profiles of toluene and C3–C6 species between baseline flames (black open symbols) and doped ones (colored full symbols) for the methane flames (left column) and the ethylene ones (right column). The computational results are plotted with colored lines for the doped flames and with black lines for the baseline flames. Continuous line are for Metcalfe-Mech [35] and dashed line for Ranz-Mech [36]. (For interpretation of the references to color in this figure legend, the reader is referred to the web version of this article.)

centrations of propene and C_3H_4 are approximately 15 ppm and 25 ppm, respectively. The concentration maxima are located at about 5.5 mm from the fuel nozzle, that is, where toluene decay is the largest. The maximum concentrations of propene and C_3H_4 in the baseline flame are much lower at about 3.5 ppm, indicating that both derive from toluene cracking. The concentration of propene computed with the Metcalfe-Mech in the baseline flame is higher than that computed for the doped flame, with the latter a factor of two larger than the experimental values. Ranzi-Mech behaves comparably, predicting even higher concentrations. Both models also predict concentrations of C_3H_4 lower than the measured values in the doped flame and higher in the baseline flame, with higher concentrations in the baseline flame in contrast with the experimental results.

Therefore, neither model seems to reproduce accurately the pathway yielding C3 species from toluene cracking in the methane flame. This finding confirms that the mechanism of benzyl radical ring opening is not sufficiently well established [52–54]. Two global unimolecular reactions proposed by Colket and Serry [16] and generating cyclopentadienyl, acetylene, C_3H_3 and C_4H_4 , are often used, but Jones et al. [52] demonstrated theoretically that the rate constants for these pathways have not been properly evaluated. Thus, these two reactions do not seem to describe the cracking of benzyl radical and to account for the variety of fragments that can be generated.

The concentration profiles of propene and C_3H_4 in the ethylene flames are not significantly affected by toluene addition, since they are already generated in significant amounts in the baseline flame and are part of the fixed pool in which toluene consumption occurs. In contrast with the methane flame case, both models quantitatively predict propene and C_3H_4 in the ethylene flames. Ranzi-Mech also confirms that they are not affected by toluene addition, whereas Metcalfe-Mech predicts propene concentration slightly higher (15%) for the baseline flame.

Isobutane, normal butane, butene, without distinguishing between the iso and n-isomers, 1,3-butadiene, labeled as C_4H_6 by lumping eventual contributions of butyne and butadiene, vinylacetylene (C_4H_4) and biacetylene (C_4H_2) were also experimentally detected in the investigated flames. The concentration of iso- and n-butane are always lower than 1 ppm, as predicted for all flames by Ranzi-Mech and for methane flame by Metcalfe-Mech. The latter predicted concentration of butanes as high as 6 ppm and 2.5 ppm in the baseline and in the doped ethylene flame, respectively.

Butene was not detected in the methane flames, even if the models predict few ppm (1 or 2) to be generated independently of toluene addition, the computed concentration being slightly larger in the baseline flame. Butene was detected with concentration from 4 ppm to 7 ppm in the doped ethylene flame in the region between 4.5 and 5.5 mm, that is where toluene consumption was experimentally observed to occur. Butene concentration in the baseline ethylene flame is about three times lower clearly indicating that it is generated from toluene consumption. Both models fail in reproducing this behavior since they predict butene concentration (iso and normal have been added) to be higher in the baseline flame compared to the doped one. This behavior is particularly pronounced for the Metcalfe-Mech and the predicted concentration in the baseline flame is as high as the one measured in the doped flame for both models.

Butadiene, vinylacetylene and biacetylene were measured in the methane doped flame with concentrations between 3 and 5 ppm (peak at 5.5 mm) whereas they have not been detected in the methane baseline flame, similarly to what observed for propene and C_3H_4 . Both models predict their concentration to be lower than 1.5 ppm in both doped and baseline methane flame even if they are partially able to capture a concentration increase due to

toluene addition. Those C4 species are generated in much larger amounts in the ethylene doped flame and their concentrations are virtually unaffected by toluene addition, as experimentally verified and correctly reproduced by both models, with the exception of butadiene that is predicted to be sensibly higher in the baseline flame by the Metcalfe-Mech. Moreover, the Metcalfe-Mech quantitatively reproduce vinylacetylene and biacetylene concentration, but overpredicts by a factor between 3.4 and 5 butadiene concentration. On the contrary, Ranzi-Mech works much better for butadiene, but overpredicts C_4H_4 and C_4H_2 by almost a factor of three.

The inability of the models to capture accurately the formation of butadiene, vinylacetylene and biacetylene in the methane doped flame and of butene in the ethylene doped flame, is also related to the inadequate description of the aromatic ring opening mechanisms, as discussed in the context of C3 species. The experimental data reported here may help identifying future improvements to the mechanisms.

Few ppm of pentenes (also isoprene), 1,4-pentadiene and linear- C_6H_6 were also measured in the ethylene flames, but their profiles are not reported here. Among them, only pentadiene is generated from toluene decomposition and was detected only in the doped flame with a 2.5 ppm peak at 5.5 mm. Metcalfe-Mech does not include such species, whereas Ranzi-Mech predicts concentrations higher than the measured ones, being not affected by toluene addition.

Benzene and cyclopentadiene concentration profiles are grouped in a single graph as closed ring products of toluene decomposition (Fig. 5g, h), as further elaborated in subsequent figures. They are detected only in the doped flame for the methane flame cases, with concentration as high as about 40 ppm for benzene, that is the most abundant stable product of toluene decomposition, and at 5 ppm for cyclopentadiene. Both models predict almost no generation of these species in the methane baseline flame and reproduce quite well benzene profile in the doped methane flame, but at a concentration of 20% and 35% lower than the measured one for Ranzi-Mech and Metcalfe-Mech, respectively. The cyclopentadiene profile is properly reproduced by Ranzi-Mech and underpredicted by Metcalfe-Mech. It would appear that the mechanisms are able to reproduce the overall reactivity of toluene and the formation of its major products when it is not mixed with aliphatic compounds with more than two carbon atoms.

The picture is quite different for the incipiently sooting ethylene flames since relative large amounts of C3–C4 species are already generated in the baseline flame. Benzene and cyclopentadiene were measured in the ethylene baseline flame with concentrations of about 60 ppm and 40 ppm, respectively. Experimental results shows that the addition of toluene causes an increase of about 20 ppm for cyclopentadiene concentration and of about 50 ppm for benzene one. Neither mechanism is able to capture the cyclopentadiene concentration increase, Ranzi-Mech reproducing better the profile measured in the baseline flame and Metcalfe-Mech the profile measured in the doped flame. Benzene is also largely overpredicted by both models, even if both mechanisms are partially capable of capturing the benzene concentration increase associated with toluene addition. Toluene addition in ethylene flame results in an increase of about 15 ppm of both benzene and cyclopentadiene as early as at 4.5 mm from the fuel nozzle consistently with the experimentally observed toluene consumption but neither model captures this behavior.

The evidence that neither mechanism mimics adequately toluene (Fig. 4), benzene and eventually cyclopentadiene concentrations in the ethylene baseline flame, can be ascribed to difficulties in describing the mechanism of aromatic ring formation from smaller aliphatic fragments [55] as well as their consumption rate. On the other hand, the model inability to correctly reproduce the increase in benzene and cyclopentadiene concentration in the

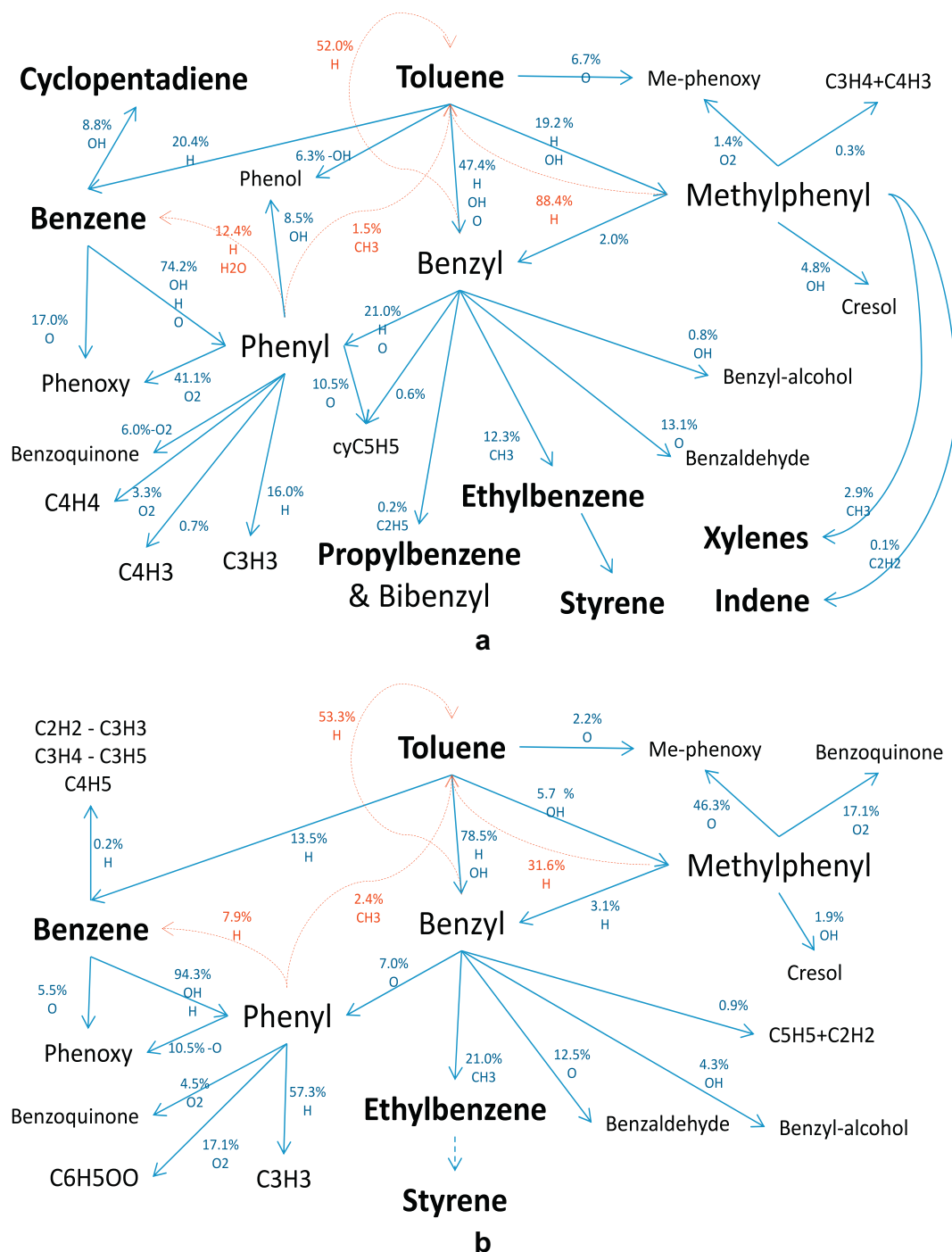


Fig. 5. Reaction path analysis for toluene destruction in the methane-doped flame: (a) Ranzi-Mech [36] and (b) Metcalfe-Mech [35]. Each arrow is labeled with principal collision partner(s) and percentage of the destruction at each step in the pyrolysis process. A few consumption steps for subsequently generated species are highlighted in red dashed lines since they result in positive production of previously generated species. Species in bold were detected and quantified in the GC-MS. (For interpretation of the references to colour in this figure legend, the reader is referred to the web version of this article.)

ethylene flame after toluene addition, is associated with the already mentioned difficulties in predicting toluene reactivity, when the toluene is in the presence of a reacting pool containing significant amounts of C₃–C₄ aliphatic species and some aromatics.

Few ppm (about 2.5 ppm) of methyl-cyclopentadiene and cyclohexadiene are also detected in the ethylene baseline flames but only the first is enhanced (1.5 time more abundant) by toluene addition. Only Ranzi-Mech includes those species, predicting negligible concentration for cyclohexadiene and almost 18 ppm of

methylcyclopentadiene for both baseline and doped flame. Benzene was also detected but not quantified, in both the baseline and the doped ethylene flame.

At this stage, in view of the partial validation of the models, with respect to some aspects of toluene pyrolytic destruction, it is interesting to perform a reaction pathway analysis at least with respect to the first few steps of the process and the eventual growth to intermediate in the soot formation process. There would be no point of following the late oxidation phase of toluene since

most of the CO and CO₂ is produced by the baseline flame. To that end, we considered first the production terms in the species equation of toluene at each location in the axial profile, divided it by the local strain rate that would account for residence time effect and sum it over the entire profile. Then we accounted only for the consumption (negative) global steps. We carried the process for the first 3 or 4 steps of the destruction “tree”, as depicted in Fig. 5a and b for the doped methane flames under consideration using both mechanisms. Each arrow in the pathway analysis is labeled with the primary collision partner(s) of the molecule in question and the percentage of the total (negative) production at that particular stage of the destruction process. A few consumption steps for subsequently generated species are highlighted in red dashed lines since they result in positive production of previously generated species. The species in bold are measured and quantified in the experiment. Ranzi-Mech predicts that toluene is attacked by the primary H–O–OH radical pool, and H in particular, that is generated in the baseline flame. That flame is well validated by the experimental measurements in Fig. 3, at least with respect to the major products. Also, since the toluene reactivity is reasonably well captured in Fig. 4, the first few steps in the toluene destruction are probably sufficiently reliable. According to Ranzi-Mech, the dominant path leads to benzyl, and eventually phenyl, with two secondary paths leading to benzene and methylphenyl, two other minor paths to Me-phenoxy and phenol through toluene attack by O and OH, respectively, both accounting for up to 13% of the toluene disappearance. Because of the proximity of the toluene decomposition region to the flame, some oxygen containing species are contributing early on to the toluene destruction path. Of the species reported in the reaction pathway analysis, only benzene was experimentally measured in the first generation of the “tree”, in reasonably good agreement with the model predictions (Fig. 4h), followed by cyclopentadiene and the aromatics in the subsequent steps, including some growth species to be discussed in the next section. The process was carried out up to oxygenated compounds such as phenol, benzaldehyde, phenoxy and benzylalcohol. Metcalfe-Mech yields a similar reaction pathway, but without the hydroxyl radical attack to phenol and with higher yield of ethylbenzene. The relative weight of the various paths also differs from Ranzi-Mech.

Turning to ethylene, we report in Fig. 6 the analogous pathway analysis. Now, the primary attack is from H alone and there is little evidence of oxidative pyrolysis in the early stages of the process, in contrast with the results in Fig. 5. This confirms the significantly different nature of the two baseline flames and the different challenges they pose to a chemical mechanism, as intended in the design of the experiments. The details of the subsequent toluene decomposition steps in the ethylene flames are probably less crucial in view of the fact that not even the overall reactivity of toluene in such flame is properly captured.

The major radicals attacking toluene (H, OH, O) are plotted in Fig. 7c and d. Whereas H is inevitably the radical diffusing the furthest upstream, the three radicals are bunched up spatially at comparable concentrations in approximately the same spatial location where they overlap with toluene decay in the case of the methane doped flame. For the ethylene flame, where the high temperature region is much further on the oxidizer side, the profiles are much better separated in the toluene consumption region, where the H radical concentration is much larger than those of the other two radicals. This spatial distribution is consistent with the path analysis in Figs. 5 and 6, with H being the dominant radical attacking toluene in the ethylene flames, and a greater role of OH and O in the methane flames, as already discussed. To shed light in the subsequent steps in the toluene pyrolysis, the figure is completed with the computed profiles of the principal radical intermediates benzyl, phenyl and methylphenyl (Fig. 7e and f), followed by the stable

oxygenates, like phenol, benzyl alcohol and benzaldehyde in the methane flame, that are the only ones computed at concentration levels above ppm. The concentration profiles of methyl, ethynyl, ethyl and propargyl radicals are also shown in Fig. 5 because of the important role they play in aromatic species formation and in the possible enhancement of toluene reactivity in the ethylene flame, since they are at significant concentrations.

5.4. Growth from toluene doping

The experimental and computational concentration profiles of species larger than toluene are summarized in Fig. 8 both for methane and ethylene flames. We identified and quantified ethylbenzene, styrene, phenylacetylene, propylbenzene, xylenes (the lumped concentration is shown, even if ortho-xylene was detected separately from the undistinguishable meta and para isomers) and indene. Some of these compounds are relevant intermediate in soot formation [56]. Naphthalene and acenaphthylene were also identified but not quantified since the shape of their profiles depended on the flame scanning direction, probably because of condensation in the sampling line. These species are generated from toluene growth, but they can be already present in the incipiently sooting baseline ethylene flame where also toluene is formed. Numerical results for all of the detected species are available only for Ranzi-Mech, since Metcalfe-Mech does not include some of the identified compounds.

Because of the abundance of methyl radical, the dominant species larger than toluene in the doped methane flame is ethylbenzene peaking between 5.0 and 5.5 mm with concentrations of about 15 ppm. It was undetected in the baseline flame. Metcalfe-Mech reproduces quite well its profile, whereas Ranzi-Mech underpredicts the maximum concentration in the doped methane flame by a factor of three. Ethylbenzene mainly forms through benzyl and methyl radical recombination [19] as shown in Fig. 5. Since both models give essentially identical CH₃ profiles, this result suggests that Metcalfe-Mech is able to capture benzyl formation in the doped methane flame correctly.

Trace amounts (less than 1 ppm) of ethylbenzene were also detected in the ethylene baseline flame, where the addition of toluene causes its concentration to be sensibly higher by about 4.5 ppm. Neither mechanism performs well in the ethylene flames, since Metcalfe-Mech largely overpredicts concentrations in the baseline flame and Ranzi-Mech underpredicts concentrations in the doped flame, neither capturing the right increase in ethylbenzene concentration due to toluene addition. The discrepancy with the models is particularly pronounced between 4.5 mm and 5 mm, that is the region where experimental toluene concentration starts to drop. Once again, this discrepancy underlies the inability of models to reproduce toluene reactivity in the ethylene flame, since the benzyl radical concentration must be underpredicted by at least a factor of three to account for the surplus of ethylbenzene generated because of toluene addition. Moreover, an additional pathway could be active to explain the discrepancy between 4.5 and 5 mm, since the methyl radical concentration is negligible small in this region (Fig. 4g). Such a pathway could involve the phenyl and ethyl radical recombination, as discussed in Fig. 6 for Ranzi-Mech.

Styrene was also detected in trace amounts (about 1 ppm) in the methane doped flame, but not in the baseline one, whereas phenylacetylene was not detected in the methane flames. Both models reproduce quite well the experimental results even if Metcalfe-Mech does not include phenylacetylene chemistry. Styrene and phenylacetylene have been detected in significant amounts, in both baseline and doped ethylene flames at about 10 ppm and 5 ppm, respectively and their concentrations are not significantly affected by toluene addition. Only styrene is slightly (by about

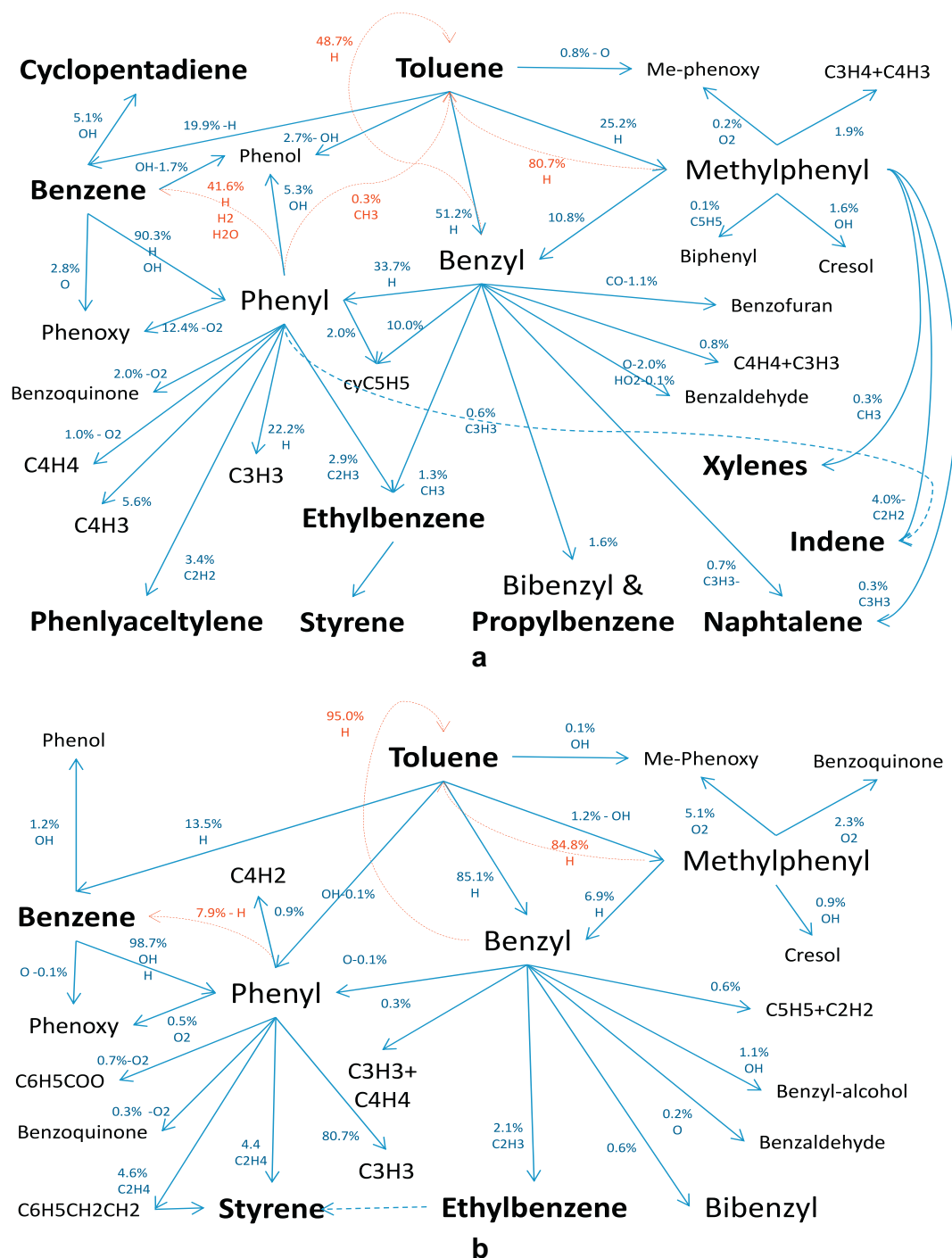


Fig. 6. Reaction path analysis for toluene destruction in the ethylene-doped flame: (a) Ranzi-Mech [36] and (b) Metcalfe-Mech [35]. Each arrow is labeled with principal collision partner(s) and percentage of the destruction at each step in the pyrolysis process. A few consumption steps for subsequently generated species are highlighted in red dashed lines since they result in positive production of previously generated species. Species in bold were detected and quantified in the GC-MS. (For interpretation of the references to colour in this figure legend, the reader is referred to the web version of this article.)

2 ppm) more abundant in the doped flame. Metcalfe-Mech overpredicts styrene concentration by a factor of approximately two in both the baseline and doped ethylene flame, predicting an increase in concentration due to toluene addition. Ranzi-Mech behaves somewhat worse, since styrene concentrations are overpredicted by a factor of 4 and phenylacetylene ones by a factor much larger than 10, phenylacetylene being also larger for the doped flame as opposed to the experimental results.

Trace amounts (about 1 ppm) of meta- and para-xylenes were detected in the methane doped flame but not in the baseline one.

Their concentrations were correctly predicted by the Ranzi-Mech as lumped xylenes and are not included in Metcalfe-Mech. Similar quantities of ortho- xylene and propyl-benzene and even smaller amounts (not quantified) of methyl-styrene and 2-propenyl-benzene were detected in the methane doped flame. Metcalfe-Mech does not include such species, whereas Ranzi-Mech include both xylenes lumped together, and propyl-benzene. This model is only able to roughly reproduce the peak position of xylenes in the ethylene flame but their concentrations are largely underpredicted. The modeled peak position of propylbenzene is slightly shifted

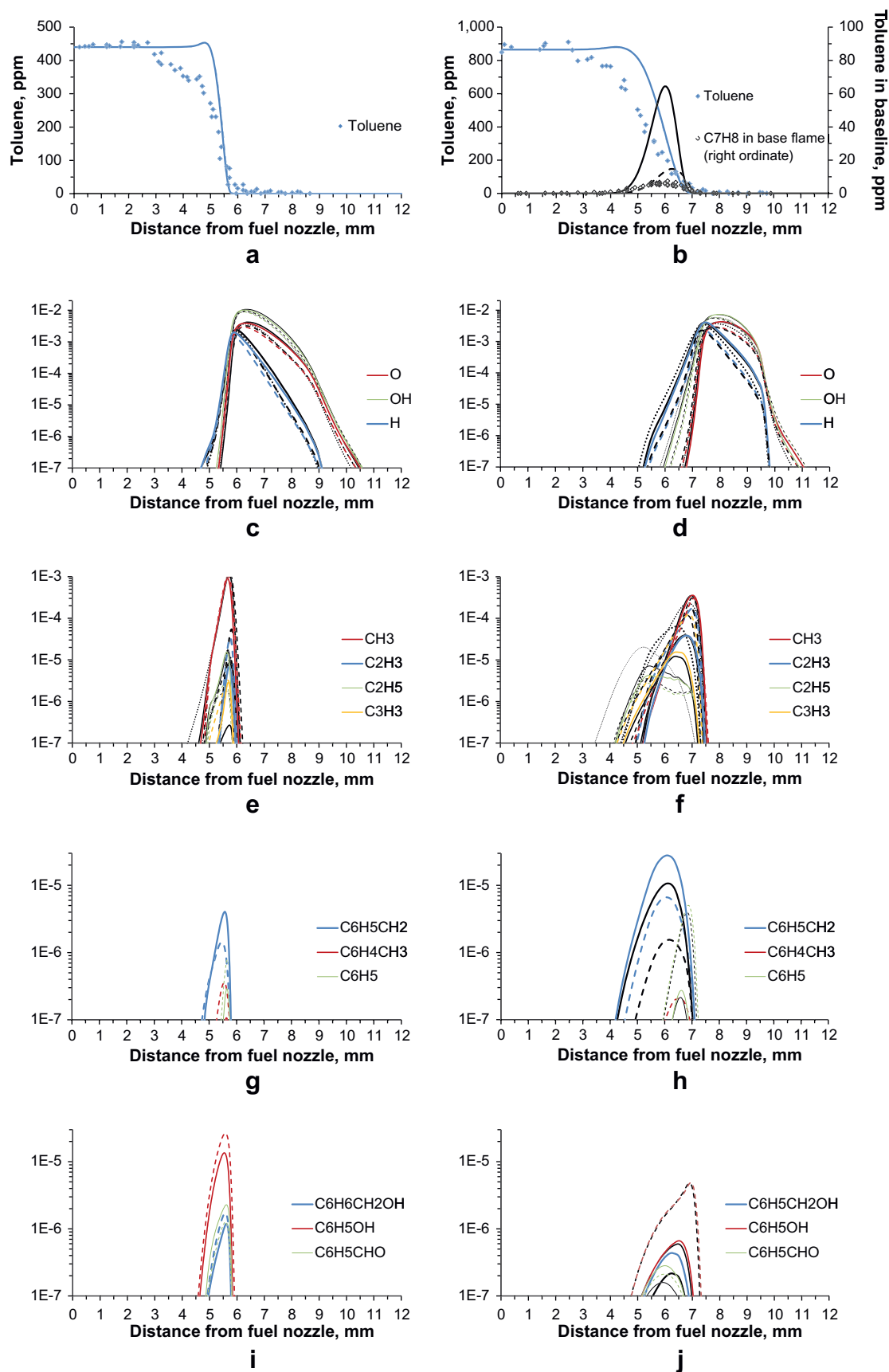


Fig. 7. Profiles of experimental and computed toluene mole fraction (a and b), computed H–O–OH radical pool (c and d), methyl–ethyl–ethynyl–propargyl– radicals (e and f), principal radical intermediates (benzyl and phenyl) (g and h) and stable oxygenates (phenol, benzyl alcohol and benzaldehyde) (i and j). The computational results are plotted in color for the doped flame and in black for the baseline flame with the same legenda as in Fig. 2 (Metcalfe-Mech [35] – dashed line and Ranzi-Mech [36] – dotted line).

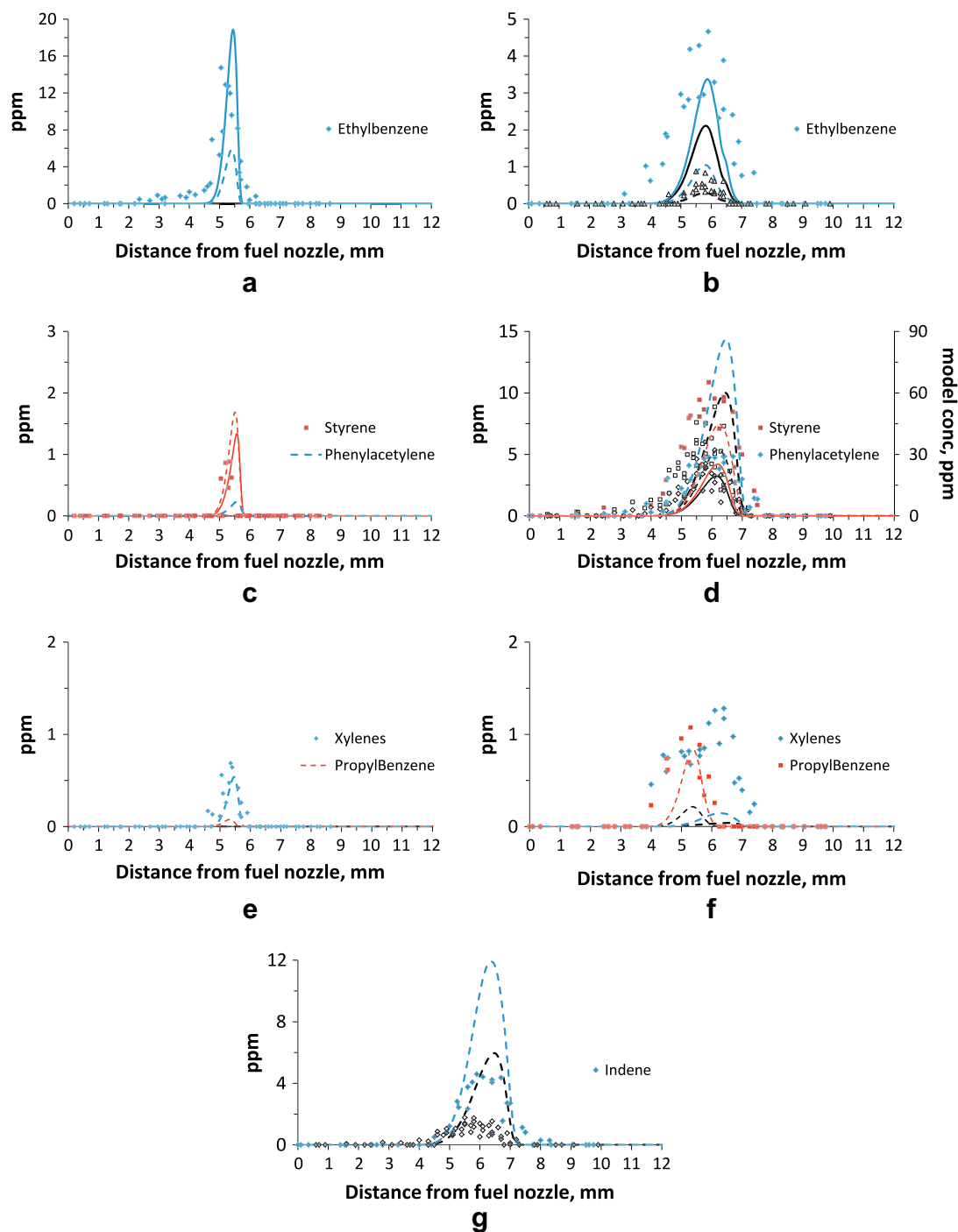


Fig. 8. Comparison of growth species between baseline flames (black open symbols) and doped ones (colored full symbols) for the methane flames (left column) and the ethylene ones (right column). The computational results are plotted with colored lines for the doped flames and with black lines for the baseline flame. Continuous lines are for Metcalfe-Mech [35] and dashed lines for Ranzi-Mech [36].

towards the oxidizer side as compared to the measurements, even if the maximum concentration is properly predicted in the doped flame. The experimental concentrations of xylenes, propylbenzene and ethylbenzene, are non-completely negligible in the region between 4.5 and 5 mm, where the models fail to predict toluene consumption.

Xylenes due to toluene addition are modeled as generated through methyl-phenyl and methyl radical recombination in Ranzi-Mech, so that methyl-phenyl concentrations should be higher than predicted for consistency with the observed discrepancy. Propyl-benzene is generated from benzyl and ethyl-radical recombination,

whereas no pathways including phenyl radical are included in Ranzi-Mech.

Perhaps the most interesting measured species in the context of soot formation in the ethylene flame is indene: the second aromatic ring formation is considered to be the bottleneck to soot formation from mono-aromatic fuels such as toluene [56]. Significant amounts (5 ppm) of indene were identified in the incipiently sooting ethylene doped flame, mostly due to toluene addition since its concentration in the baseline flame is much lower (less than 2 ppm). Small amounts of indane (less than 0.5 ppm) were also detected in the ethylene doped flame. Ranzi-Mech is able to predict

the peak position of indene and the concentration increase due to toluene addition. The model overpredicts indene concentration by a factor 5 in the baseline flame.

Traces amounts (estimated at less than 2 ppm) of naphthalene and acenaphthylene were also identified in the ethylene flames but they were not quantified. The signals for those species are not macroscopically affected by the toluene addition, consistently with the prediction of Ranzi-Mech. The latter largely overpredicts the estimated concentration of naphthalene in the ethylene baseline flame. Bibenzyl was not detected in all investigated flames, even if it is considered to be important through benzyl radical recombination [19]. Both Metcalfe-Mech and Ranzi-Mech predict small concentrations for this species, at most 2 ppm in the doped ethylene flame.

6. Conclusions

The structure of gaseous counterflow diffusion flames perturbed with the addition of hundreds of ppm of prevaporized toluene is studied in two distinct flame environments: a blue methane flame stabilized on the *fuel* side of the gas stagnation plane and an incipiently sooting ethylene flame stabilized on the *oxidizer* side of the gas stagnation plane. By GC-MS analysis of gas samples extracted from the flames, the structure of these flames is reconstructed to provide an experimental data set for the testing of chemical mechanisms in a well-controlled testbed. Profiles of critical toluene pyrolysis products and stable growth species, including ethylbenzene and indene are compared with computational models using two semi-detailed chemical mechanisms: Ranzi-Mech and Metcalfe-Mech. Principal conclusions follow:

- A. The two selected flame environments provide a well defined “reactor” in terms of temperature–time history, major species, primary H–OH–O radical pool and intermediate C2 species, all of which are unaffected by toluene doping. In addition, the gaseous ethylene flame determines the concentrations of C3 (propene, and propyne and allene lumped together) and C4 (butadiene, vinyl-acetylene and biacetylene) species, with the exception of butene, all unaffected by doping. In the methane flame, because of the proximity of the toluene decomposition region to the flame, some oxygen containing species are contributing early on to the toluene destruction path. A reaction path analysis indicate that according to Ranzi-Mech toluene is attacked by the primary H–O–OH radical pool, that is generated in the baseline flame, and H in particular. In the ethylene case, the primary attack is from H alone and there is little evidence of oxidative pyrolysis in the early stages of the process. More generally, fuel degradation occurs in an oxygen-deficient environment in the incipiently sooting ethylene flame. This confirms the significantly different nature of the two baseline flames and the different challenges they pose to the validation of a chemical mechanism, as intended in the design of the experiments. As a result, these flames environments provide a well defined platform for the testing of the interaction of toluene with different radical pools and smaller aliphatic fragments, as typical of practical fuel combustion.
- B. Experimentally, probably because of the presence of aliphatic fragments, toluene reactivity is enhanced in these flames, as compared to simpler reactive environments, with the onset of toluene decay beginning at relatively modest temperatures, on the order of 800 K. This reactivity is captured reasonably well by both chemical mechanisms in the methane flame. Not so in the ethylene flame, in the presence

of a richer, more complex mixture. This discrepancy has implications for the modeling of practically relevant fuel blends with both aliphatic and aromatic compounds;

- C. Neither model seems to reproduce accurately the pathway yielding C3 and some C4 species from toluene cracking, which implies that the aromatic ring opening mechanism appears to be inadequately described.
- D. Both models reproduce quite well benzene profile in the doped methane flame, in the presence of aliphatics containing no more than two carbon atoms, but not in the doped ethylene flame.
- E. Neither mechanism mimics adequately toluene, benzene and eventually cyclopentadiene concentrations in the ethylene baseline flame, which is symptomatic of difficulties in describing the mechanisms of aromatic ring formation from smaller aliphatic fragments as well as its opening.
- F. The reaction path analysis of toluene consumption in the doped methane flame with Ranzi-Mech indicates that the dominant path leads to benzyl, and eventually phenyl, with two secondary paths leading to benzene and methylphenyl. Two other paths yielding Me-phenoxy and phenol through toluene attack by O and OH, respectively, account for up to 13% of the toluene disappearance. Metcalfe-Mech yields a similar reaction pathway, but without the hydroxyl radical attack to phenol. The relative weight of the various paths also differs between the two mechanisms.
- G. Because of the abundance of methyl radical, the dominant species larger than toluene in the doped methane flame is ethylbenzene. Metcalfe-Mech reproduces quite well its profile, whereas Ranzi-Mech underpredicts the maximum concentration. This result suggests that Metcalfe-Mech is able to capture benzyl formation in the doped methane flame correctly.
- H. Perhaps the most interesting measured species in the context of soot formation in the ethylene flame is indene, since the second aromatic ring formation is considered to be the bottleneck to soot formation from monoaromatic fuels. Ranzi-Mech is able to predict the peak position of indene and the concentration increase due to toluene addition, but overpredicts indene concentration in the baseline flame.
- I. The experimental data reported here may help identifying future improvements to the mechanisms. For example, toluene can be attacked by radicals other than the major ones and it could interact also with stable species. The methylphenyl radical should be generated in larger amount from toluene pyrolysis to justify the formation of xylenes, and so on.

Acknowledgments

The authors gratefully acknowledge: the financial support of AFOSR (Grant #FA9550-06-1-0018, Dr. Julian Tishkoff, Program Manager), the technical assistance of Mr. Lorenzo Figura in the implementation of the thin filament pyrometry, Drs. Alessio Frassoldati and Alberto Cuoci in Professor Ranzi's group at Politecnico di Milano for providing the executable of the openSMOKE code that was used in preliminary calculations.

References

- [1] T. Edwards, L.Q. Maurice, J. Propul. Power 17 (2001) 461–466.
- [2] C.P. Wood, V.G. McDonell, R.A. Smith, G.S. Samuelson, J. Propul. Power 5 (1989) 399–405.
- [3] W.D. Shultz, ACS Petrol. Chem. Div. Preprints 37 (1991) 383–392.
- [4] A. Violi, E.G. Eddings, A.F. Sarofim, S. Granata, T. Faravelli, E. Ranzi, Combust. Sci. Technol. 174 (2002) 399–417.

- [5] A. Agosta, N.P. Cernansky, D.L. Miller, T. Faravelli, E. Ranzi, *Exp. Therm. Fluid Sci.* 28 (2004) 701–708.
- [6] P. Dagaut, A. El Bakali, A. Ristori, *Fuel* 85 (2006) 944–956.
- [7] S. Humer, A. Frassoldati, S. Granata, T. Faravelli, E. Ranzi, R. Seiser, K. Seshadri, *Proc. Combust. Inst.* 31 (2007) 393–400.
- [8] S. Honnet, K. Seshadri, U. Niemann, N. Peters, *Proc. Combust. Inst.* 32 (2009) 485–492.
- [9] S. Dooley, S.H. Won, M. Chaos, J. Heyne, Y. Ju, F.L. Dryer, K. Kumar, C.J. Sung, H. Wang, M.A. Oehlschlaeger, R.J. Santoro, T.A. Litzinger, *Combust. Flame* 157 (2010) 2333–2339.
- [10] J.M. Simmie, *Prog. Energy Combust. Sci.* 29 (2003) 599–634.
- [11] P. Dagaut, M. Cathonnet, *Prog. Energy Combust. Sci.* 32 (2006) 48–9292.
- [12] F. Battin-Leclerc, *Prog. Energy Combust. Sci.* 34 (2008) 440–498.
- [13] W.J. Pitz, C.J. Muller, *Prog. Energy Combust. Sci.* 37 (2011) 330–350.
- [14] W.J. Pitz, N.P. Cernansky, F.L. Dryer, F.N. Egolfopoulos, J.T. Farrell, D.G. Friend, H. Pitsch, Development of an Experimental Database and Chemical Kinetic Models for Surrogate Gasoline Fuels, SAE Technical Paper, 2007, 2007-01-0175.
- [15] K. Brezinsky, T.A. Litzinger, I. Glassman, *Int. J. Chem. Kinet.* 16 (1984) 1053–1074.
- [16] M.B. Colket, D.J. Seery, *Proc. Combust. Inst.* 25 (1994) 883–891.
- [17] S.D. Klotz, K. Brezinsky, I. Glassman, *Proc. Combust. Inst.* 27 (1998) 337–344.
- [18] P. Dagaut, G. Pengloan, A. Ristori, *Phys. Chem. Chem Phys.* 4 (2002) 1846–1854.
- [19] R. Bounaceur, I. Da Costa, R. Fournet, F. Billaud, F. Battin-Leclerc, *Int. J. Chem. Kinet.* 37 (2004) 25–49.
- [20] R. Sivaramakrishnan, R.S. Tranter, K. Brezinsky, *Combust. Flame* 139 (2004) 340–350.
- [21] Y. Sakai, H. Ozawa, T. Ogura, A. Miyoshi, M. Koshi, W.J. Pitz, Effects of Toluene Addition to Primary Reference Fuel at High Temperature, SAE, 2007, 2007-01-4104.
- [22] H.-P.S. Shen, J. Vanderover, M.A. Oehlschlaeger, *Proc. Combust. Inst.* 32 (2009) 165–172.
- [23] V. Detilleux, J. Vandooren, *J. Phys. Chem. A* 113 (2009) 10913–10922.
- [24] A. Hamins, K. Seshadri, *Combust. Flame* 68 (1987) 295–307.
- [25] A. Hamins, D.T. Aderson, J.H. Miller, *Combust. Sci. Technol.* 71 (1990) 175–195.
- [26] A. El Bakali, L. Dupont, B. Lefort, N. Lamoureux, J.F. Pauwels, M. Montero, *J. Phys. Chem. A* 111 (2007) 3907–3921.
- [27] T. Zhang, L. Zhang, X. Hong, K. Zhang, F. Qi, C.K. Law, T. Ye, P. Zhao, Y. Chen, *Combust. Flame* 156 (2009) 2071–2083.
- [28] Y. Li, L. Zhang, Z. Tian, T. Yuan, J. Wang, B. Yang, F. Qi, *Energy Fuels* 23 (2009) 1473–1485.
- [29] L. Tosatto, B. La Mantia, H. Bufferand, P. Duchaine, A. Gomez, *Proc. Combust. Inst.* 32 (2009) 1319–1326.
- [30] H. Bufferand, L. Tosatto, B. La Mantia, M.D. Smooke, A. Gomez, *Combust. Flame* 156 (2009) 1594–1603.
- [31] S. Jahangirian, C.S. McEnally, A. Gomez, *Combust. Flame* 156 (2009) 1799–1809.
- [32] C.J. Sun, C.J. Sung, H. Wang, C.K. Law, *Combust. Flame* 107 (1996) 321–335.
- [33] A.E. Lutz, R.J. Kee, J.F. Grcar, F.M. Rupley, Sandia Laboratory, Report MS-9042, SAND96-8243, 1996.
- [34] http://me.berkeley.edu/gri_mech/version30/text30.html.
- [35] W.K. Metcalfe, S. Dooley, F.L. Dryer, *Energy Fuels* 25 (2011) 4915–4936.
- [36] <http://creckmodeling.chem.polimi.it/kinetic.html>.
- [37] T. Bieleveld, A. Frassoldati, A. Cuoci, T. Faravelli, E. Ranzi, U. Niemann, K. Seshadri *Proc. Combust. Inst.* 32 (2009) 493–500.
- [38] G. Chen, A. Gomez, *Combust. Flame* 110 (1997) 392–404.
- [39] R.H. Natelson, M. Kurman, N.P. Cernansky, D.L. Miller, *Fuel* 87 (2008) 2339–2342.
- [40] C. Shaddix, K. Brezinsky, I. Glassman, *Proc. Combust. Inst.* 24 (1992) 683–690.
- [41] R.G. Butler, I. Glassman, *Proc. Combust. Inst.* 32 (2009) 395–402.
- [42] V. Vilimpoc, L.P. Goss, *Proc. Combust. Inst.* 22 (1988) 1907–1914.
- [43] L. Figura, A. Gomez, *Combust. Flame* 159 (2011) 142–150.
- [44] L.V. King, *Philos. Trans. Roy. Soc. London, Ser. A* 214 (1914) 373–433.
- [45] A. Cuoci, A. Frassoldati, T. Faravelli, E. Ranzi, in: *Proceedings of the 34th Meeting of the Italian Section of the Combustion Institute, Italy, October 24–26, 2011*.
- [46] K. Seshadri, F.A. Williams, *Int. J. Heat Mass Transfer* 21 (1978) 251–253.
- [47] C.J. Sung, J.B. Liu, C.K. Law, *Combust. Flame* 102 (1995) 481–492.
- [48] I.K. Puri, K. Seshadri, M.D. Smooke, D.E. Keyes, *Combust. Sci. Technol.* 56 (1987) 1–22.
- [49] B.A.V. Bennet, C.S. McEnally, L.D. Pfefferle, M.D. Smooke, M.B. Colcket, *Combust. Flame* 127 (2001) 2004–2022.
- [50] G. Vanhove, G. Petit, R. Minetti, *Combust. Flame* 145 (2006) 521–532.
- [51] Y. Sakai, A. Miyoshi, M. Koshi, W.J. Pitz, *Proc. Combust. Inst.* 32 (2009) 411–418.
- [52] J. Jones, G.B. Bacskay, J.C. Mackie, *J. Phys. Chem. A* 101 (1997) 7105–7113.
- [53] G. da Silva, J.A. Cole, J.W. Bozzelli, *J. Phys. Chem. A* 113 (2009) 6111–6120.
- [54] D. Polino, A. Famulari, C. Cavallotti, *J. Phys. Chem. A* 115 (2011) 7928–7936.
- [55] C.S. McEnally, L.D. Pfefferle, B. Atakan, K. Kohse-Hoinghaus, *Prog. Energy Combust. Sci.* 32 (2006) 247–294.
- [56] C.S. McEnally, L.D. Pfefferle, *Combust. Flame* 148 (2007) 210–222.